Research paper

Molecular modeling on transportation of CO_2 in montmorillonite: Diffusion and permeation

Haixiang Hu[*], Yanfei Xing, Xiaochun Li

State Key Laboratory of Geomechanics and Geotechnical Engineering, Institute of Rock and Soil Mechanics, Chinese Academy of Sciences, Wuhan, Hubei 430071, China

ARTICLE INFO

ABSTRACT

CO_2 storage in underground saline aquifers is helpful to reduce CO_2 emission in the atmosphere, where gas/fluid diffusion and permeation in clay mineral plays a key role in CO_2 leakage and underground migration. CO_2 Permeability and different fluid diffusivities in clay mineral (montmorillonite, Mt) interlayers are investigated by molecular dynamics (MD). Both CO_2 and H_2O self-diffusivities increase with water concentration and temperature but show a maximum at the CO_2 concentration of 2 molecule/unit-cell unconventionally. The fractional free volume of Mt increases with CO_2 concentration but begins to decrease if CO_2 concentration exceeds 2, thus giving the reason for the above unusual CO_2 self-diffusivity variation. Displacement distribution of CO_2 molecules is found to be characterized by logarithmic normal distribution. The mean value of such distribution further supports the self-diffusivity dependence on CO_2 concentration. M-S and Fick diffusivities of CO_2 are positively related to CO_2, H_2O concentration and temperature. CO_2 permeability is calculated by MD for the first time, which increases with CO_2 pressure and H_2O concentration but exhibits a turning point at temperature 360 K due to low CO_2 solubility at high temperature.

1. Introduction

CO_2 storage in underground saline aquifers provides long-term and large-scale storage of CO_2, which is a promising way to reduce CO_2 emission in the atmosphere. In this process, clay minerals, such as illite, chlorite, kaolinite, and montmorillonite (Mt) (Josh et al., 2012), are the main components of caprocks. Owing to their porous (layered) structure, the clay minerals have remarkable capacity of adsorbing CO_2 (Fu et al., 1990; Khosrokhavar et al., 2014). On the other hand, clay mineral has a low permeability and therefore the clay-enriched caprocks show excellent sealing ability to retain injected CO_2 (Abdou and Ahmaed, 2010; Gaus, 2010; Gernot et al., 2013). Gas leakage and environmental impacts are the most concerned problems for risk assessments of CO_2 storage, which are closely related to fluid (gas) transportation (diffusion and permeation) in clay mineral.

The interactions of CO_2 and clay mineral have been reported by many authors. For example, Giesting et al. investigated impact of CO_2 absorption on Ca-exchanged Mt expansion under different CO_2 pressure (Giesting et al., 2012). CO_2 can migrate the interlayer region of montmorillonite based on the in situ X-ray diffraction (XRD), magic angle spinning nuclear magnetic resonance spectroscopy (NMR) and attenuated total reflection infrared spectroscopy (ATR) (Loring et al., 2014; Loring et al., 2012). In addition, quasi-elastic neutron scattering

experiments (QENS) experiments on hydrated clays have shown that hydrated cation diffusion mobility is probably a complex dynamic process and the diffusion coefficients of the exchangeable cations were estimated (Sobolev et al., 2009). Kozaki et al. determined the apparent diffusion coefficients of Cs^+ as functions of the temperature (Kozaki et al., 1999). Sánchez et al. discussed that the self-diffusion of water depended on temperature and ionic strength in different kinds of clays (Sánchez et al., 2008). However, there are a few experiments on diffusivity of CO_2 in clay although permeation processes in sediments and clay-rich rocks have been investigated experimentally by many authors (Javadpour et al., 2007). For instance, permeability of CO_2 declined during shearing while increasing sliding velocity reduced the decline rate (Javadpour, 2009). Permeability of simulated granite is highly related to fracture transmissivity (Tanikawa et al., 2014).

Molecular simulation becomes a powerful tool in many fields and has been used for understanding the molecular-scale structural (Lee et al., 2014; Teich-Mcgoldrick et al., 2015), thermodynamic (Boek et al., 1995), mechanical (Zhang et al., 2015), and dynamic (Botan et al., 2010; Krishnan et al., 2013; Malikova et al., 2004; Yang and Zhang, 2005) properties of clay mineral. Grand canonical Monte Carlo (GCMC) method was applied to simulation the adsorption of CO_2 with H_2O (Botan et al., 2010), CH_4 (Jin and Firoozabadi, 2013; Kadoura et al., 2016; Yang et al., 2015), and organic molecules (Krishnan et al.,

---

2013; Yu et al., 2003) in Mt. Molecular dynamics (MD) was employed to study the structure and self-diffusion coefficient of carbon dioxide in uncharged clay-like slit pores (Yang and Zhang, 2005). Cygan et al. developed CLAYFF force field (Cygan et al., 2004) for clay mineral and three-site flexible potential modes of CO_2 (Cygan et al., 2012). Botan et al. demonstrated that CO_2 considerably influenced the diffusion of mobile species in clay minerals (Botan et al., 2010). Myshakin et al. showed that the intercalation of CO_2 in Mt caused the significant changes of the d-spacing and described that the distribution and diffusion of CO_2, H_2O, Na^+ was affected by the number of layers of clay mineral (Makaremi et al., 2015; Myshakin et al., 2014; Myshakin et al., 2013).

Although fluid self-diffusion coefficients (SDC) in clay mineral has been investigated by MD and macroscopic permeability have been discussed experimentally in some of above works, the other transportation diffusivities and permeability of CO_2 have not been explored microscopically by MD yet. MD study on various diffusion coefficients and permeability of CO_2 in clay mineral, Mt, will be performed in this work. The effects of gas concentration, water concentration, and temperature are considered.

2. Methods

2.1. Theoretic aspects

Self-diffusion means random motions or mixing of particles at the thermodynamic equilibrium. SDC, D_{iself}, of component i is computed by Einstein equation

$$D_{iself} = \frac{1}{2dn_i} \lim_{t \to \infty} \frac{d}{dt} \sum_{l=1}^{n} (r_{l,i}(t) - r_{l,i}(0))^2 \tag{1}$$

where n_i is the number of the molecules of the component i, d is the dimension of the system, and $r_{l,i}(t)$ is position vector of the molecule l at time t.

Fick diffusion is characterized by the particle motions driven by concentration gradient, leading to the net mass transport. Fick's law of diffusion defines the transport diffusivity or Fick diffusion coefficient (FDC), D_{iFick}, as the proportionality factor between the flux N and the concentration c gradient:

$$N_i = -D_{iFick} \nabla c_i \tag{2}$$

Chemical potential gradient is considered as the fundamental driving force for diffusion (Krishna, 2012; Krishna and Jasper, 2005). For a single component diffusion in porous material the transport equation can be expressed as

$$N_i = -L_i \nabla \mu_i \tag{3}$$

where μ_i is the chemical potential of gas i. L is obtained from the MD simulations using (Theodorou et al., 1996)

$$L_i = \frac{1}{2dVk_B T} \lim_{\Delta t \to \infty} \frac{1}{\Delta t} \left\langle \left(\sum_{l=1}^{n_i} (r_{l,i}(t + \Delta t) - r_{l,i}(t)) \right)^2 \right\rangle \tag{4}$$

where V is the Mt volume, k_B is the Boltzmann constant and T is the temperature. The content in < ... > means an average on the cross displacement correlation function (CDCF). The notation < > represents an average on a number of independent particle ensembles rather than single particles.

Using Maxwell-Stefan (M-S) theory (Maxwell, 1867; Stefan, 1871), the diffusion formula of single component follows

$$N_i = -\rho \Theta_{i,sat} D_{iM-S} \frac{\theta_i}{k_B T} \nabla \mu_i \tag{5}$$

where ρ is the Mt density expressed as the number of unit cells per cubic meter, $\Theta_{i,sat}$ is the saturation loading of the component i, μ_i is the chemical potential expressed in Joules per molecule. N_i is the molar flux of

the component i expressed in molecules per square meter per second, the fractional occupancy θ_i is defined as

$$\theta_i = \frac{\Theta_i}{\Theta_{i,sat}} \tag{6}$$

where Θ_i is the loading of the component i. Combing the Eq. (3) and Eq. (5), the Maxwell-Stefan diffusion coefficient (MDC), D_{iM-S}, is calculated by

$$D_{iM-S} = \frac{k_B T}{\rho \Theta_i} L_i \tag{7}$$

Under isothermal condition, the molecules are considered to move with average velocity subject to a driving force $\nabla \mu_j$, $\mu = \mu_0 + k_B T \ln f$, where f is the fugacity, then $\nabla \mu = k_B T \nabla f / f$, so that Eq. (2) is equivalent to Eq. (3).

$$N_i = -\rho D_{iFick} \nabla c_i = -\rho D_{iFick} \nabla \Theta_i = -\rho D_{iFick} \Theta_i \frac{\partial \ln \Theta_i}{\partial \ln f_i} \frac{\nabla \mu_i}{k_B T} \tag{8}$$

The FDC and MDC are related by

$$D_{iFick} = D_{iM-S} \Gamma \tag{9}$$

where Γ is the thermodynamic factor

$$\Gamma = \Theta_i \frac{\partial \ln f_i}{\partial \Theta_i} \tag{10}$$

Permeability, P, measures the ability of fluids (gas or liquid) to flow through porous media. Solubility coefficient, S, is an important factor to determine the thermodynamic behavior (adsorption) of the fluid in porous media, which are defined as:

$$S = c/f, \ P = D_{iM-S} S \tag{11}$$

Following the derivation given by Konstantinos Makrodimitris et al. (Makrodimitris et al., 2001), P can be calculated from:

$$P = -\frac{D_{iM-S}}{\Delta f} \int_{f_1}^{f_2} \frac{c(f)}{f} df \tag{12}$$

where c is the concentration in porous media as a function of fugacity, f_1 and f_2 are downstream and upstream pressure in the permeability determination respectively.

2.2. Molecular dynamics simulation details

The sodium-saturated Wyoming-type Mt is used as the clay mineral crystal model with unit formula $Na_{0.5}[Si_8](Al_{3.5}Mg_{0.5})O_{20}(OH)_4$ (Skipper et al., 1995), which comprises the 2:1 or tetrahedral − octahedral − tetrahedral (TOT) layers. The substitutions of octahedral Al^{3+} by Mg^{2+} lead to net negative layer charge. The interlayer Na^+ cations are balanced by these negative changes. Three-dimensional periodic boundary condition is applied to a simulation box composed of 32 (8 × 4 × 1) unit cells. Mt model with different number of CO_2 and H_2O are allowed to freely swell to their equilibrium d-spacing. All simulated systems are listed in Table 1. Cn ($n = 1, 2, …$) denote the system in which the number of H_2O is fixed and the number of CO_2 is represented by n. Hn (n = 1,3, …) represent systems with different number of H_2O. Tn (n = 1,2, …) mean systems with varying temperature.

All simulations are performed with the Accelrys Material Studio software (http://accelrys.com/). The CLAFF force field is used {Cygan, 2004 #42}. The Ewald summation method is applied to the electrostatic interaction. The atom-based summation method is used in the van der Waals interactions. Gas diffusions are simulated as follows: gases are first inserted into the above equilibrium configuration by grand canonical Monte Carlo (GCMC) method to get a new clay-gas cell. The cell is minimized and equilibrated by NPT and NVT runs. Then the cell runs in an NVT ensemble (0.5 ns) followed by a long-time (5 ns) NVE run. The trajectories in the NVE run are saved for diffusion coefficient

Table 1
Details of simulated systems. Number in bracket indicates the corresponding CO_2 or H_2O concentration in molecules/cell.

Number of CO_2	Number of H_2O	Temperature	d-Spacing	Short-name
10 (0.331)	160 (5)	313.15	12.50	C1
16 (0.5)	160 (5)	313.15	12.70	C2
32 (1)	160 (5)	313.15	13.50	C3
48 (1.5)	160 (5)	313.15	14.00	C4
64 (2)	160 (5)	313.15	14.50	C5
80 (2.5)	160 (5)	313.15	14.75	C6
64 (2)	32 (1)	313.15	11.90	H1
64 (2)	96 (3)	313.15	13.00	H3
64 (2)	160 (5)	313.15	14.50	H5
64 (2)	224 (7)	313.15	15.50	H7
64 (2)	288 (9)	313.15	17.25	H9
32 (1)	128 (4)	273.15	12.50	T1
32 (1)	128 (4)	313.15	12.50	T2
32 (1)	128 (4)	353.15	12.50	T3
32 (1)	128 (4)	393.15	12.50	T4
32 (1)	128 (4)	433.15	12.50	T5

computation. Integration time step is set to 1 fs. Gas concentration, water component and temperature are varied to investigate their impacts on gas diffusions.

3. Results and discussion

3.1. SDC

Molecular dynamics (MD) simulation can be used to obtain not only gas diffusion coefficients but also the microscopic details of the diffusion process, which is helpful to understand underlying diffusion mechanism in a confined space. Diffusion coefficients are calculated based on statistically averaging the motion of large amounts of particles, and their accuracy relies on the sample size. Each system is run ten times independently to get reliable results. The resulting MSDs are averaged to calculate SDC. Note that Unless stated otherwise, the diffusion coefficients in this paper refer to that of diffusion in the x-y plane. MSD_{xy} of the C4 system varies with time is taken as an example (Fig. 1). MSD_{xy} displays a good linear correlation with time. The SDC can then be determined using eq.(1). The resulting SDC is 7.584×10^{-10} m^2 s^{-1} for CO_2 in the C4 system, which is close to the result of Myshakin et al. (2013). The SDC of CO_2 in Mt is lower than that of CO_2 in pure water, 2.93×10^{-9} m^2 s^{-1} (Tamimi et al., 1994), which is due to the confinement effect of Mt interlayer surface. Diffusion coefficients are related to many factors including type and concentration of the gas, pore size, temperature and so on. Injection pressure of CO_2, moisture content and underground temperature are key factors in the geological storage of CO_2.

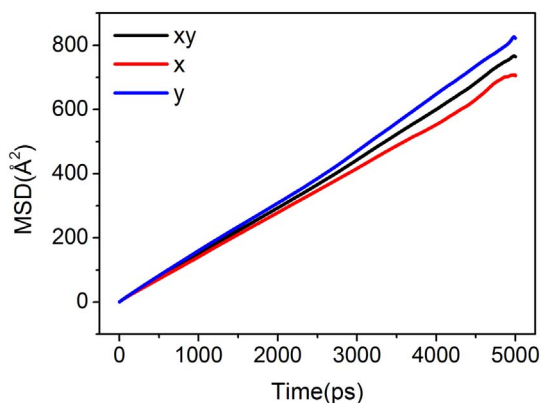The influence of CO_2 concentration on its SDC is considered first.

Fig. 1. The average MSD vs time in C4 system.

The number of water molecules is set to 5 molecules per unit cell and the temperature to 313.15 K (approximately the temperature of 1000 m underground). The Monte Carlo method is used to insert varying amounts of CO_2 molecules into the system. The system is then relaxed to equilibrium through NPT and NVT run, with resulting interlayer distances (d-spacing) shown in Table 1. The equilibrated system is then subject to dynamic run in NVE ensemble to compute SDC, as shown in Fig. 2(a). With the increase of CO_2 concentration, the SDCs of CO_2 and H_2O first increase and then decrease. At the CO_2 loading value of 64 (C6 system), the SDCs of both reach maximum values. The SDC of H_2O remains higher than that of CO_2, which originates from the smaller thermodynamic diameter of H_2O (2.65 Å) compared with that of CO_2 (3.3 Å).

However, many studies have shown the SDCs of gases in porous media to decrease with the increase of their concentrations (Krishna and Paschek, 2002; Skoulidas and Sholl, 2005; Skoulidas et al., 2003), which is different from the aforementioned result in Fig. 2(a). In order to explore the reason for the variation of SDC, the effect of CO_2 on the Mt structure is further analyzed. As shown in Table 1, the d-spacing of Mt continues to increase with CO_2 concentration, which could provide fluids with larger space for diffusion, resulting in larger diffusion coefficient. It may be expected that SDC should increase with CO_2 concentration monotonously. However, our simulations reveal a lower SDC in high-concentration system C6 compared to the low-concentration system C5. In order to explore the reason for this unusual SDC variation further, fractional free volume (FFV) of the system which is defined as the ratio of interlayer space unoccupied by fluids to the total volume of Mt:

$$FFV = \frac{V_{free}}{V_{total}} \tag{13}$$

where V_{free} is the free (unoccupied) volume in the Mt interlayers, and V_{total} is the total volume of the simulated Mt cell. The FFV can be determined by molecular probes (Connolly, 1983; Ronova et al., 2003). FFV increases with the CO_2 concentration first and peaks at 64 CO_2 molecules also, which is in accordance with the position of the maximum of CO_2 SDC (Fig. 3(a)). This indicates two counter-interactions: first, the increase of CO_2 concentration could cause the expansion of d-spacing in the system and provide fluids with more space for diffusion; on the other hand, the increase of CO_2 molecules occupies more space, resulting in a decrease of free volumes. The fluid molecules become more crowded and diffuse more slowly. Therefore, fluid SDC depends on the free space in the interlayer. At the initial stage of CO_2 injection, the rapid expansion of d-spacing raises the free volume in the interlayer, which is beneficial for fluid diffusion, and causes CO_2 SDC to increase; the free volume reaches a maximum at 64 CO_2 molecules; the free volume decreases despite the continued expansion of d-spacing, which hinders gas diffusion and causes descending SDCs of CO_2 and H_2O (Fig. 3(a)).

Water is the most important geological fluid and water content varies with the location and the depth of storage aquifer. A Mt system with 2CO_2 molecules per unit cell is used to investigate quantitatively the impact of water concentration on the diffusion. Temperature is fixed at 313 K. SDCs of both CO_2 and H_2O increase with H_2O concentration (Fig. 2(b)). Similarly, the FFVs under different moisture contents can be calculated. FFV increases with moisture content (Fig. 3(b)), showing the same trend as the SDCs. This indicates the increase of water molecules raises the free volume in the interlayer space and contributes to the fluid diffusion.

At last, temperature is considered. As shown in Fig. 2(c), the increase of temperature can accelerate the thermal motion of molecules and then increase their kinetic energy, causing the fluid SDC to increase gradually. It is revealed that the relationship between SDC and temperature follows the classical Arrhenius formula:
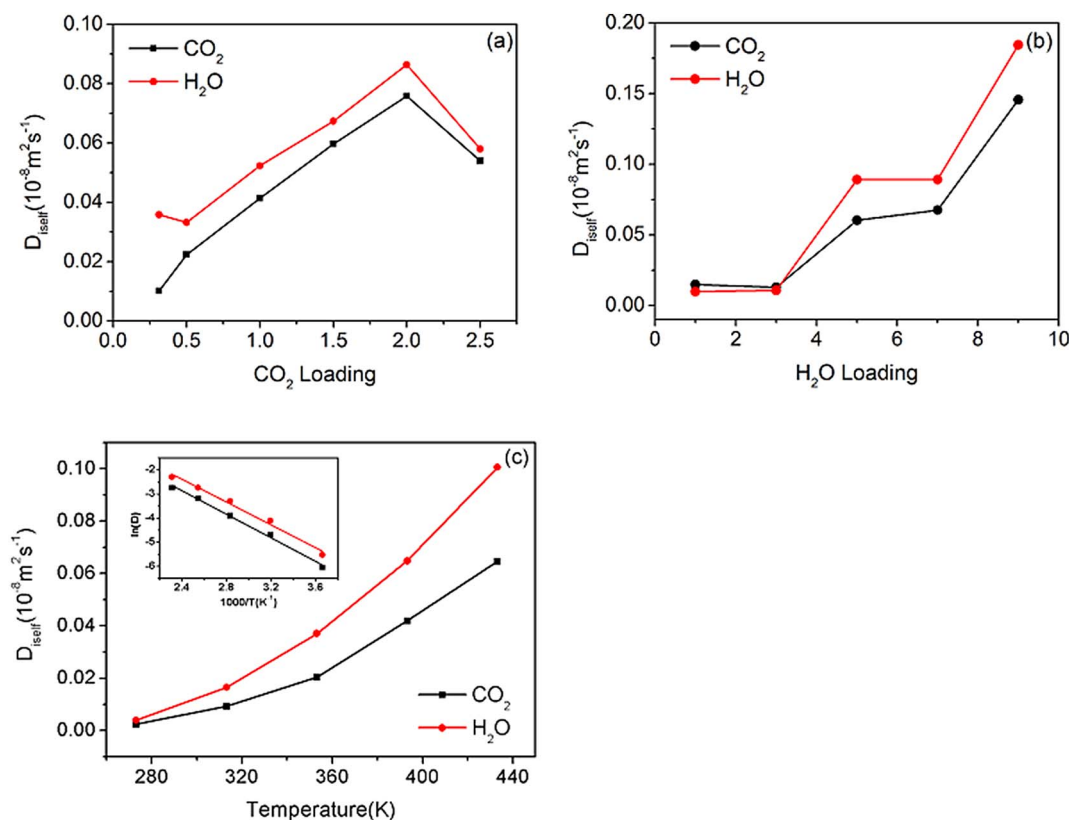
$$D = D_0 e^{-\frac{E_a}{RT}} \tag{14}$$

Fig. 2. The self-diffusion coefficient D_{iself} of CO_2 and H_2O in Mt variation with: (a) CO_2 loading, (b) H_2O loading and (c) temperature. Inset of (c) shows Arrhenius plot of SDC versus temperature.

where D_0 is a constant, and E_a is the activation energy of diffusion. According to the equation, the activation energy for CO_2 diffusion in Mt is 20.26 kJ/mol (see Fig. 2(c)), which is greater than its activation energy of diffusion in pure water 17.8904 kJ/mol (Tamimi et al., 1994). This implies the Mt layers impose restriction on CO_2 diffusion, leading to a higher activation energy in Mt.

MD can provide more details such as the paths and displacements of molecules to study the microscopic mechanism of gas diffusion. Since layered Mt provides anisotropic confined space without interconnected micropores, diffusion of gas in such structure is different from random movements of gas in unlimited environment. The displacement distribution of CO_2 molecules is further analyzed. All the distributions have single peak and no peak is shown at large displacements (Fig. 4). The displacements generally fall within the 0.6–1.0 Å. As CO_2 concentration increases, the displacement peak (i.e. the prevailing displacement) moves toward the right and becomes wider, reaching the maximum width in the C5 system (Fig. 4(a)). This indicates increases of both the prevailing displacement and the number of fast-speed molecules. Therefore, with the increase of CO_2 concentration, SDC of CO_2

increases and reaches a maximum at C5 system. Similarly, the increase of moisture and temperature lead to both increase of prevailing displacement and peak width, causing the SDC to increase (Fig. 4(b)–(c)). The displacement distributions can be fitted to logarithmic normal distribution function (LNDF):

$$y = \frac{e^{-\frac{(-a+\log[x])^2}{2b^2}}}{d\sqrt{2\pi}x}$$ (15)

The curves are well-fitted with the data ($R^2 > 0.98$) (Fig. 5(a)). To quantitatively examine the relationship between the displacement distribution and SDC, the mean value of LNDF: $R_{av} = e^{(a + b^2/2)}$ (unit Å), an important characteristic parameter for log-normal distributions, is calculated (Fig. 5(b)–(d)). Here R_{av} increases with CO_2 concentration firstly, reaches a maximum at C5, and then decreases (Fig. 5(b)), showing the same trend as the SDC of CO_2. The average displacement of molecules in unit time (1 ps) reflects the relative speed of diffusion and hence larger R_{av} results in faster diffusion rate and a higher SDC. In a word, R_{av} is positively related to the SDCs of CO_2 and H_2O. This is

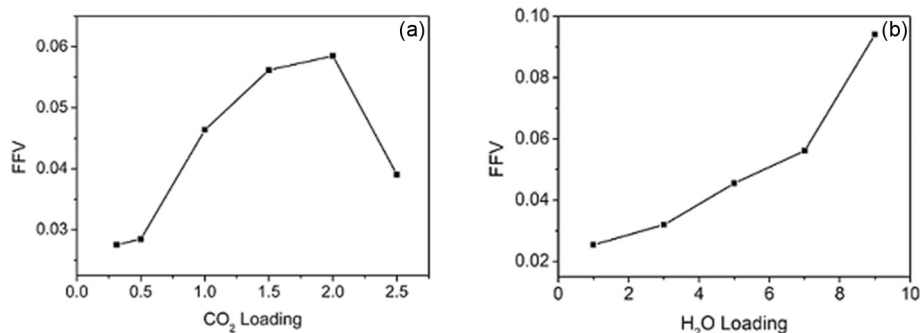**Fig. 3.** FFV dependence on: (a) CO_2 loading, (b) H_2O loading.
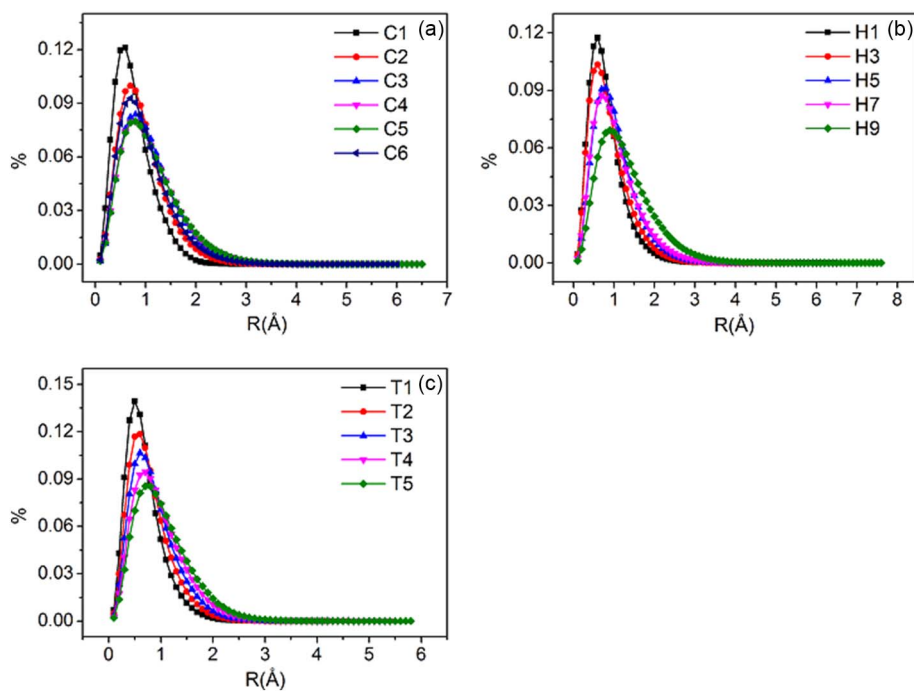
Fig. 4. The distribution of displacement in different systems: (a) CO_2 loading, (b) H_2O loading, (c) temperature.

further validated by systems with varying moisture content and temperatures. As Shown in Fig. 5(c) and (d), R_{av} increases with moisture, and increases linearly with temperature, causing the increase of SDCs of CO_2 and H_2O (Fig. 2).

3.2. MDC and FDC

The Onsager coefficient L should be determined using Eq. (4) first to get MDC. Note that, unlike the MSD in Eq. (1) which measures single particle movement, CDCF in Eq. (4) measures the collective motion of all fluid molecules in Mt. Displacement summation of all the particles

within time interval Δt is calculated first. Then the average of the square of the summation plotted against time, whose slope is used to get L according to Eq. (4). This formula not only applies to single fluid diffusion but also suits multi-component fluid diffusion (Hu et al., 2017). There is a good linear correlation between CDCF and time (Fig. 6). L can thus be computed from the slope of the curve, which is used to get MDC from Eq. (7) and FDC using Eq. (9). It is noted that the thermodynamic factor in Eq. (9) requires the adsorption isotherm of CO_2 which can usually be simulated using the GCMC method. The conventional GCMC method assumes a rigid adsorbent (μVT ensemble). However, it is known that Mts wells after adsorbing CO_2. Swollen Mt
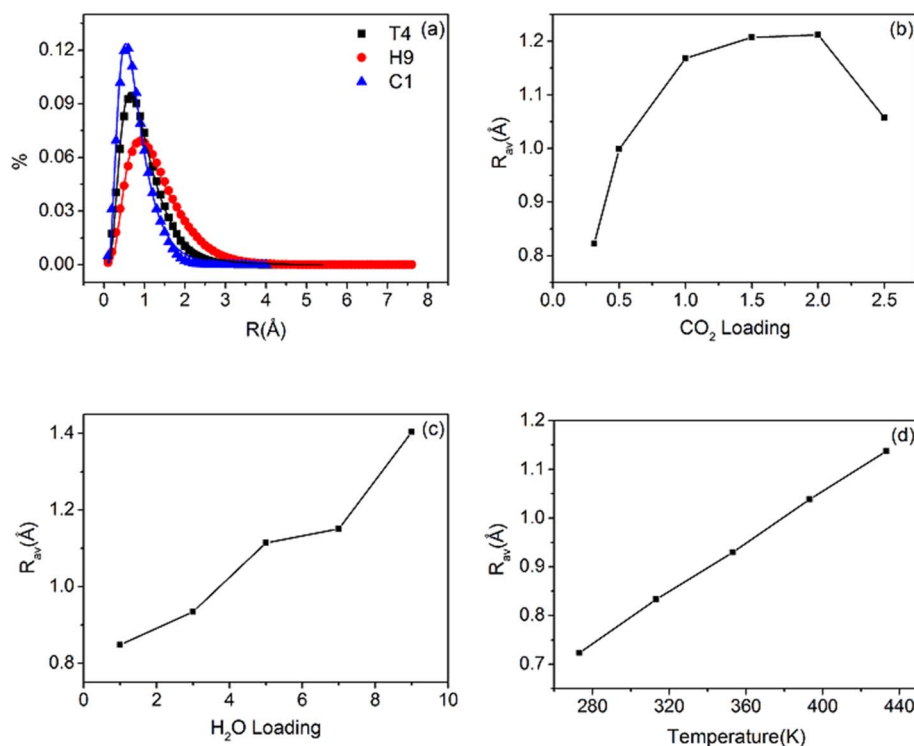

Fig. 5. (a) The distributions of CO_2 displacement, and the lines are fitted by logarithmic normal distribution. The mean value of distribution in different systems: (b) CO_2 loading, (c) H_2O loading, (d) temperature.
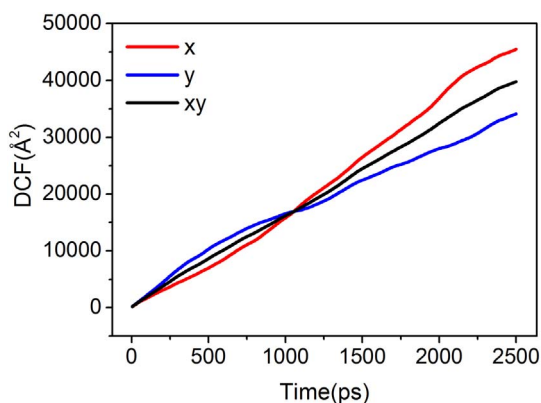
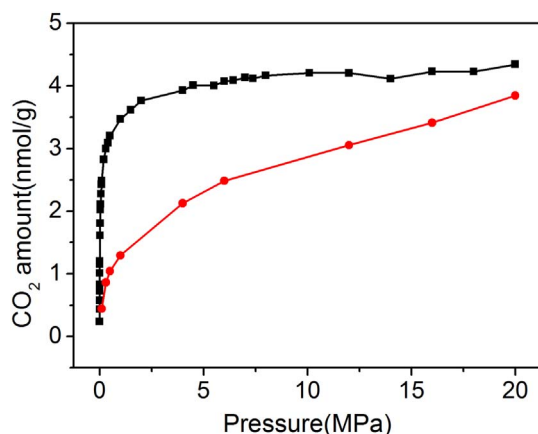**Fig. 6.** The average CDCF vs time in C4 system.

Fig. 7. Adsorption isotherms of CO_2 by conventional GCMC method (black) and flexible adsorption method (red) in C1 system. (For interpretation of the references to colour in this figure legend, the reader is referred to the web version of this article.)

can continue to absorb more gas. Therefore, the conventional GCMC is not suitable for calculating adsorption isotherms of CO_2 in Mt. Here a new elastic-adsorption approach is adopted to simulate CO_2 isotherm by taking into account the swelling of Mt. The Mt structure with the initial 224 water molecules is taken as an example for comparison (Fig. 7). Using the conventional GCMC method, one can obtain significantly different adsorption isotherms at different fixed d-spacing values, i.e., the initial d-spacing and swollen d-spacing. In these isotherms, the curves rapidly approach to saturation at low pressure, and the amount of CO_2 adsorption almost keeps constant when the pressure rises above 1 MPa (shown by the black curve in Fig. 7), which is inconsistent with experimental results (Busch et al., 2008). However, the CO_2 adsorption isotherm obtained by the above elastic-adsorption method increases gradually with the CO_2 pressure, which is more qualitatively coincident with the Langmuir formula and the above-
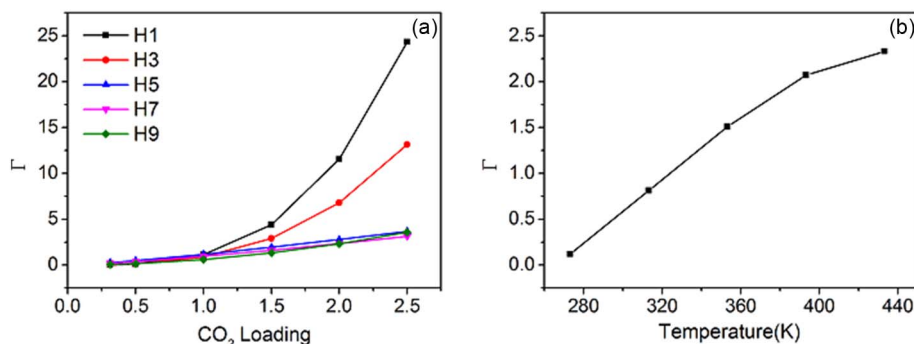
mentioned experiment results. The maximum adsorption θ_{sat} is obtained by fitting the Langmuir equation, from which the thermodynamic factor can be calculated by Eq. (10). Thermodynamic factor always increases with CO_2 concentration (Fig. 8(a)); for low CO_2 concentrations, thermodynamic factor is not influenced by H_2O apparently, while for higher CO_2 concentrations, the thermodynamic factor gradually decreases with H_2O content. In a system with 128 H_2O molecules and 32 CO_2 molecules, the higher temperature leads to the larger thermodynamic factor (Fig. 8(b)).

The effects of CO_2 concentration, H_2O content and temperature on MDC and FDC are also examined. The red dots in Fig. 9 represent the variation of CO_2 MDC, which increase with CO_2 concentration, H_2O content and temperature. The black dots in Fig. 9 indicate the FDC. Since the thermodynamic factor is generally above unit, the FDC is usually larger than MDC. Similar to MDC, FDC increases with CO_2 concentration, H_2O content and temperature. This means that CO_2 diffuses faster with the increase of storage depth because of higher CO_2 injection pressure and higher temperature. CO_2 pressure and temperature will decrease with CO_2 diffusing toward ground surface, leading to slower diffusion of CO_2.

3.3. Permeability

Based on the above results of MDC and adsorption isothermals, permeability of CO_2 can be computed through Eq. (12). Note that CO_2 permeability under different CO_2 pressure can be computed from a single adsorption isothermal but multiple CO_2 adsorption isothermals are needed for CO_2 permeability at various H_2O content and temperature. Generally, the permeability of CO_2 in Mt interlayer is very small (Fig. 10), on the order of 10^{-12}–10^{-13} Mol/(m·s·Pa). Permeability depends on gas fugacity. In civil engineering, gas permeability is usually correlated to pressure. Here the CO_2 concentration is converted into CO_2 pressure based on adsorption isothermals. As shown in Fig. 10(a), CO_2 permeability first increases sharply at relatively low CO_2 pressure (pressure < 7 MPa) and tends to reach saturation at high pressure. This originates from the Langmuir type of CO_2 adsorption isothermal which goes up quickly with CO_2 pressure at low pressure and saturates at high pressure. Meanwhile, permeability increases with H_2O content exponentially (Fig. 10(b)): namely P increase gradually at low H_2O content but goes up more sharply at higher H_2O content. However, dependence of permeability on temperature shows different behavior (Fig. 10(c)). CO_2 permeability rises with temperature initially, reaching maximum at 360 K, and decreases once temperature is higher than 360 K. From Eq. (11), permeability is related to both MDC and solubility The turning point results from the decrease of solubility at high temperature, although D_{iM-S} monotonously increases with temperature. From the above, it can be concluded that CO_2 permeability is mainly determined the behavior of solubility parameter because MDC just varies in a limited range. As the increase of storage site depth, CO_2 should be injected with higher pressure and underground temperature increases. It is expected that CO_2 permeates faster with depth increasing

Fig. 8. The thermodynamic factor dependence on CO_2 loading (a) and temperature (b) In the system with 128 H_2O molecules and 32 CO_2 molecules.
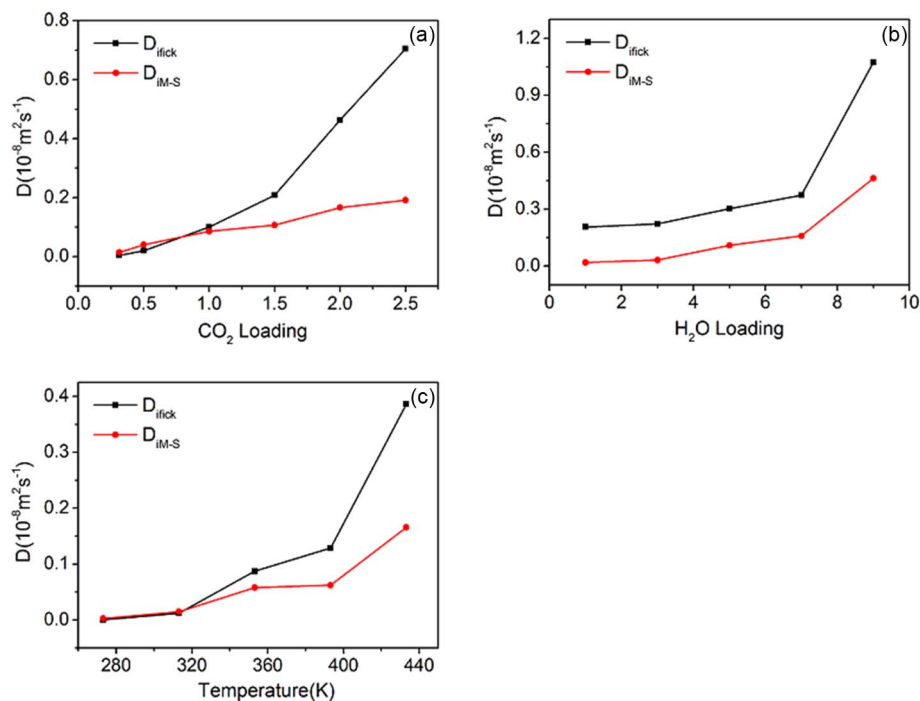
Fig. 9. The D_{iM-S}, D_{ifick} of CO_2 variation with: (a) CO_2 loading, (b) H_2O loading, (c) temperature.

if storage depth is < 3000 m (around 360 K), but CO_2 permeability could decrease once the depth exceeds 3000 m because CO_2 permeability almost keeps stable for high CO_2 concentration while CO_2 permeability goes down at high temperature. Note that compared with temperature and CO_2 concentration, water content is relatively steady with the depth increase in a specific geologic condition. As to CO_2 storage engineering, it is recommended that less-humidity storage site should be preferred and the storage depth should be < 3000 m to reduce CO_2 leakage.

4. Conclusions

CO_2 diffusion and permeation in Mt under varying conditions is investigated by MD. The results show that while both water content and temperature are positively correlated to the SDC, the SDCs of CO_2 and H_2O display a peak with the increase of CO_2 concentration. To explain the unusual findings of the SDC further, FFV within Mt and the displacement distribution of CO_2 is analyzed. It is found that FFV has an important effect on the diffusion of gas molecules in Mt. The increase of CO_2 concentration causes the Mt to expand, increasing the internal FFV of Mt and providing gas molecules with more space for diffusion. This explains the initial increase of the fluid SDC in Mt. FFV begins to
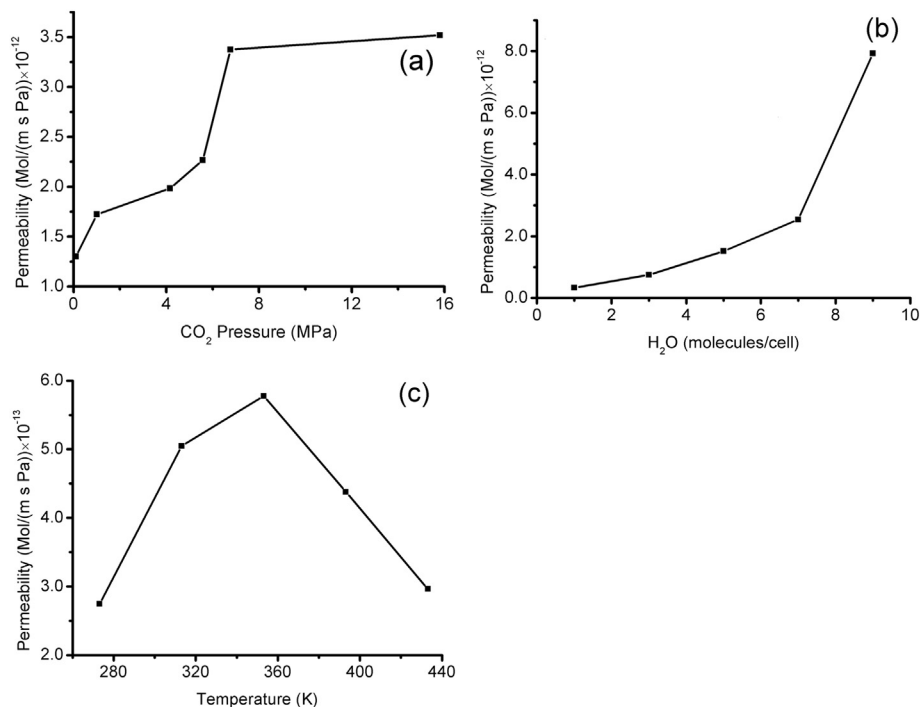

Fig. 10. Dependence of CO_2 permeability on CO_2 pressure (a), water content (b) and temperature (c).

decrease when the CO_2 concentration rises above 2 molecules/unit cell, which hinders the gas diffusion and therefore leads to decreasing SDC. Similarly, the increase of water content also causes the Mt to expand and creates more free space for CO_2 diffusion, resulting in increasing CO_2 SDC. It can be drawn that SDC of the fluid in Mt depends on the FFV of Mt. Furthermore, the displacement distribution of CO_2 follows log-normal distribution, and the mean of the distribution shows the same trend as the SDC, which provides a good explanation of the effects of CO_2 concentration, moisture and temperature on SDC from another perspective.

MDC and FDC increase with CO_2 concentration, moisture and temperature. Based on the aforementioned M-S diffusivities, CO_2 permeability under different conditions is calculated by MD for the first time. CO_2 permeability increases with CO_2 pressure and H_2O content but displays a maximum at temperature 360 K due to decreasing CO_2 solubility at high temperature. This work could provide basic transportation parameters to estimate CO_2 leakage and assess environmental risk of CO_2 underground storage in aquifer.

Acknowledgements

References

Abdou, M.I., Ahmaed, H.E., 2010. Evaluation of low-solids mud reological behavior during drilling shale formation and their effect on the pay zone productivity. Pet. Sci. Technol. 28, 934–945.

Boek, E.S., Coveney, P.V., Skipper, N.T., 1995. Monte Carlo molecular modeling studies of hydrated li-, Na-, and K-smectites: understanding the role of potassium as a clay swelling inhibitor. J. Am. Chem. Soc. 117, 12608–12617.

Botan, A., Rotenberg, B., Marry, V., Turq, P., Noetinger, B., 2010. Carbon dioxide in montmorillonite clay hydrates: thermodynamics, structure, and transport from molecular simulation. J. Phys. Chem. C 114, 14962–14969.

Busch, A., Alles, S., Gensterblum, Y., Prinz, D., Dewhurst, D., Raven, M., Stanjek, H., Krooss, B., 2008. Carbon dioxide storage potential of shales. Int. J. Greenh. Gas Control 2, 297–308.

Connolly, M.L., 1983. Solvent-accessible surfaces of proteins and nucleic acids. Science 221, 709–713.

Cygan, R.T., Liang, J.J., Kalinichev, A.G., 2004. Molecular models of hydroxide, oxyhydroxide, and clay phases and the development of a general force field. J. Phys. Chem. B 108, 1255–1266.

Cygan, R.T., Romanov, V.N., Myshakin, E.M., 2012. Molecular simulation of carbon dioxide capture by montmorillonite using an accurate and flexible force field. J. Phys. Chem. C 116, 13079–13091.

Fu, M.H., Zhang, Z.Z., Low, P.F., 1990. Changes in the properties of a montmorillonite-water system during the adsorption and desorption of water: Hysteresis1. Clay Clay Miner. 38, 485–492.

Gaus, I., 2010. Role and impact of CO_2–rock interactions during CO_2 storage in sedimentary rocks. Int. J. Greenh. Gas Control 4, 73–89.

Gernot, R., Ilton, E.S., Dirk, W., Thomas, H., Schaef, H.T., Odeta, Q., Rosso, K.M., Felmy, A.R., Krukowski, E.G., Stack, A.G., 2013. CO_2 sorption to subsingle hydration layer montmorillonite clay studied by excess sorption and neutron diffraction measurements. Environ. Sci. Technol. 47, 205–211.

Giesting, P., Guggenheim, S., Groos, A.F.K.V., Busch, A., 2012. X-ray diffraction study of K- and Ca-exchanged montmorillonites in CO_2 atmospheres. Environ. Sci. Technol. 46, 5623–5630.

Hu, H., Du, L., Xing, Y., Li, X., 2017. Detailed study on self- and multicomponent diffusion of CO_2-CH4 gas mixture in coal by molecular simulation. Fuel 187, 220–228.

Javadpour, F., 2009. Nanopores and apparent permeability of gas flow in mudrocks (shales and siltstone). J. Can. Pet. Technol. 48, 16–21.

Javadpour, F., Fisher, D., Unsworth, M., 2007. Nanoscale Gas Flow in Shale Gas Sediments.

Jin, Z., Firoozabadi, A., 2013. Methane and carbon dioxide adsorption in clay-like slit pores by Monte Carlo simulations. Fluid Phase Equilib. 360, 456–465.

Josh, M., Esteban, L., Piane, C.D., Sarout, J., Dewhurst, D.N., Clennell, M.B., 2012. Laboratory characterisation of shale properties. J. Pet. Sci. Eng. 88–89, 107–124.

Kadoura, A., Narayanan Nair, A.K., Sun, S., 2016. Adsorption of carbon dioxide, methane, and their mixture by montmorillonite in the presence of water. Microporous Mesoporous Mater. 225, 331–341.

Khosrokhavar, R., Wolf, K.H., Bruining, H., 2014. Sorption of CH4 and CO_2 on a carboniferous shale from Belgium using a manometric set-up. Int. J. Coal Geol. 128,
153–161.

Kozaki, T., Sato, H., Sato, S., Ohashi, H., 1999. Diffusion mechanism of cesium ions in compacted montmorillonite. Eng. Geol. 54, 223–230.

Krishna, R., 2012. Diffusion in porous crystalline materials. Chem. Soc. Rev. 41, 3099–3118.

Krishna, R., Jasper, V.B., 2005. Diffusion of alkane mixtures in zeolites: validating the Naxwell-Stefan formulation using MD simulations. J. Phys. Chem. B 109, 6386–6396.

Krishna, R., Paschek, D., 2002. Verification of the Maxwell-Stefan theory for diffusion of three-component mixtures in zeolites. Chem. Eng. J. 87, 1–9.

Krishnan, M., Saharay, M., Kirkpatrick, R.J., 2013. Molecular dynamics modeling of CO_2 and poly(ethylene glycol) in montmorillonite: the structure of clay–polymer composites and the incorporation of CO_2. J. Phys. Chem. C 117, 20592–20609.

Lee, M.S., Mcgrail, B.P., Glezakou, V.A., 2014. Microstructural response of variably hydrated ca-rich montmorillonite to supercritical CO_2. Environ. Sci. Technol. 48, 8612–8619.

Loring, J.S., Schaef, H.T., Turcu, R.V., Thompson, C.J., Miller, Q.R., Martin, P.F., Hu, J., Hoyt, D.W., Qafoku, O., Ilton, E.S., 2012. In situ molecular spectroscopic evidence for CO_2 intercalation into montmorillonite in supercritical carbon dioxide. Langmuir 28, 7125–7128.

Loring, J.S., Ilton, E.S., Jeffrey, C., Thompson, C.J., Martin, P.F., Pascale, B., Rosso, K.M., Felmy, A.R., Schaef, H.T., 2014. In situ study of CO_2 and H_2O partitioning between Na–montmorillonite and variably wet supercritical carbon dioxide. Langmuir 30, 6120–6128.

Makaremi, M., Jordan, K.D., Guthrie, G.D., Myshakin, E.M., 2015. Multiphase Monte Carlo and molecular dynamics simulations of water and CO_2 intercalation in montmorillonite and beidellite. J. Phys. Chem. C 119.

Makrodimitris, K., Papadopoulos, G.K., Theodorou, D.N., 2001. Prediction of permeation properties of CO_2 and N2 through silicalite via molecular simulations. J. Phys. Chem. B 105, 777–788.

Malikova, N., Marry, V., Dufrêche, J.F., Turq, P., 2004. Na/Cs montmorillonite: temperature activation of diffusion by simulation. Curr. Opin. Colloid Interface Sci. 9, 124–127.

Maxwell, J.C., 1867. On the dynamical theory of gases. Proc. R. Soc. Lond. 15, 167–171.

Myshakin, E.M., Saidi, W.A., Romanov, V.N., Cygan, R.T., Jordan, K.D., 2013. Molecular dynamics simulations of carbon dioxide intercalation in hydrated Na-montmorillonite. J. Phys. Chem. C 117, 11028–11039.

Myshakin, E.M., Makaremi, M., Romanov, V.N., Jordan, K.D., Guthrie, G.D., 2014. Molecular dynamics simulations of turbostratic dry and hydrated montmorillonite with intercalated carbon dioxide. J. Phys. Chem. A 118, 7454–7468.

Ronova, I.A., Rozhkov, E.M., Alentiev, A.Y., Yampolskii, Y.P., 2003. Occupied and accessible volumes in glassy polymers and their relationship with gas permeation parameters. Macromol. Theory Simul. 12, 425–439.

Sánchez, F.G., Loon, L.R.V., Gimmi, T., Jakob, A., Glaus, M.A., Diamond, L.W., 2008. Self-diffusion of water and its dependence on temperature and ionic strength in highly compacted montmorillonite, illite and kaolinite. Appl. Geochem. 23, 3840–3851.

Skipper, N.T., Chang, F.R.C., Sposito, G., 1995. Monte Carlo simulation of interlayer molecular structure in swelling clay minerals. I: methodology. Clay Clay Miner. 43, 285–293.

Skoulidas, A.I., Sholl, D.S., 2005. Self-diffusion and transport diffusion of light gases in metal-organic framework materials assessed using molecular dynamics simulations. J. Phys. Chem. B 109, 15760–15768.

Skoulidas, A.I., Sholl, D.S., Krishna, R., 2003. Correlation effects in diffusion of CH4/CF4 mixtures in MFI zeolite. A study linking MD simulations with the Maxwell − Stefan formulation. Langmuir 19, 7977–7988.

Sobolev, O., Forestier, L.L., González, M.A., Russina, M., Kemner, E., Cuello, G.J., Charlet, L., 2009. Hydration of Na^+, Ni^{2+}, and SM^{3+} in the interlayer of hectorite: a quasielastic neutron scattering study. J. Phys. Chem. C 113, 13801–13812.

Stefan, J., 1871. Uber das Gleichgewich und die Bewegung, insbesondere die Diffusion von Gasmengen. Sitzungsber Akad Wiss Wien. 63, 63–124.

Tamimi, A., Rinker, E.B., Sandall, O.C., 1994. Diffusion coefficients for hydrogen sulfide, carbon dioxide, and nitrous oxide in water over the temperature range 293–368 K. J. Chem. Eng. Data 39, 330–332.

Tanikawa, W., Tadai, O., Mukoyoshi, H., 2014. Permeability changes in simulated granite faults during and after frictional sliding. Geofluids 14, 481–494.

Teich-Mcgoldrick, S.L., Greathouse, J.A., Jové-Colón, C.F., Cygan, R.T., 2015. Swelling properties of montmorillonite and beidellite clay minerals from molecular simulation: comparison of temperature, interlayer cation, and charge location effects. J. Phys. Chem. C 119, 20881–20891.

Theodorou, D.N., Snurr, R.Q., Bell, A.T., 1996. Molecular dynamics and diffusion in microporous materials. Compr. Supramol. Chem. 7, 507–548.

Yang, X., Zhang, C., 2005. Structure and diffusion behavior of dense carbon dioxide fluid in clay-like slit pores by molecular dynamics simulation. Chem. Phys. Lett. 407, 427–432.

Yang, N., Liu, S., Yang, X., 2015. Molecular simulation of preferential adsorption of CO_2 over CH4 in Na-montmorillonite clay material. Appl. Surf. Sci. 356, 1262–1271.

Yu, C.H., Newton, S.Q., Norman, M.A., Schäfer, L., Miller, D.M., 2003. Molecular dynamics simulations of adsorption of organic compounds at the clay mineral/aqueous solution Interface. Struct. Chem. 14, 175–185.

Zhang, W., Hu, H., Li, X., Fang, Z., 2015. Interplay of montmorillonite–H_2O–scCO2 system between mechanical behavior and adsorption: molecular dynamics. J. Phys. Chem. C 119, 21959–21968.